BIOMECHANICAL CONTROL-ALGORITHM FOR A NOVEL CONCEPT OF A HARDWARE-IN-THE-LOOP (S-)PEDELEC TEST BENCH

Sebastian Feldmann[1] and Matthias Wiedenmann[1]

[1]Department of Mechanical Engineering and Material Science, Aalen University, Germany
Sebastian.Feldmann@HS-Aalen.de, Matthias.Wiedenmann@HS-Aalen.de,

ABSTRACT

CONVENTIONAL PEDELEC TEST BENCHES FAIL TO REPLICATE THE BIOMECHANICAL COMPLEXITY OF HUMAN PEDALING, PRODUCING DAMAGE PATTERNS THAT DIFFER FROM FIELD FAILURES. THIS PAPER PRESENTS THE PROCEEDINGS OF THE DEVELOPMENT OF A HARDWARE-IN-THE-LOOP CONTROL CONCEPT FOR A BIOMECHANIC PEDELEC TESTBENCH INTEGRATING A DIGITAL TWIN OF BOTH RIDER AND ENVIRONMENT, FINALIZED IN THE YEAR 2020. THE RIDER MODEL GENERATES PHYSIOLOGICALLY REALISTIC TORQUE PROFILES INCLUDING PHASE-SHIFTED LEFT-RIGHT ACTUATION AND STANDING PEDALING WITH RADIAL BOTTOM BRACKET LOADS. UNLIKE CONVENTIONAL APPROACHES PRESCRIBING FIXED TRAJECTORIES, VEHICLE DYNAMICS EMERGE FROM RIDER-SPECIMEN-ENVIRONMENT INTERACTION. VALIDATION THROUGH 20,000 KM ENDURANCE TESTING DEMONSTRATES REPRODUCTION OF FIELD-RELEVANT FAILURE MODES—INCLUDING MICRO-CRACKS AND PITTING—UNATTAINABLE WITH TRADITIONAL PROTOCOLS.

KEYWORDS

BIOMECHANICAL CONTROL, TORQUE ACTUATION, PEDAL FORCE SIMULATION, REAL-TIME CONTROL, E-BIKE TESTING

1. INTRODUCTION

The global market for electrically assisted bicycles, commonly referred to as PedEleCs (Pedal Electric Cycles), has experienced unprecedented growth over the past decade. With annual production volumes exceeding 1.1 million units in Germany alone and continued double-digit growth rates, the pedelec industry has evolved from a niche market to a significant segment of the mobility sector [1]. This rapid expansion has brought with it engineering challenges comparable to those faced by the automotive industry, particularly regarding drivetrain reliability, durability testing, and quality assurance at scale production levels. Unlike conventional bicycles, pedelecs operate as hybrid drive systems where the rider's pedaling effort is supplemented by an electric motor. The European legal framework mandates that motor assistance be proportional to the rider's torque input and limited to speeds below 25 km/h for standard pedelecs (250W nominal power) or 45 km/h for S-Pedelecs (up to 4000W peak power at four times the pedal power) [2]. This regulatory requirement fundamentally shapes the drivetrain architecture: the pedal torque serves as the control input for the motor's power contribution, necessitating sophisticated torque sensing and power management within the central drive unit.

The verification of pedelec drivetrain durability presents unique challenges that distinguish it from conventional powertrain testing. Traditional dynamometer-based test benches typically apply constant or stepped load profiles to evaluate component fatigue life. However, such approaches fail to capture the biomechanical complexity of human pedaling, Fig. 1, which exhibits characteristic sinusoidal torque variations, phase-shifted loading between left and right pedals, and significant variations in pedaling technique across different riding conditions [3]. Furthermore, demanding riding scenarios such as standing pedaling (commonly termed

‘Wiegeschritt’, engl. ‘swaying step’) introduce substantial lateral forces and housing deformations that can reach up to 0.45 mm at the gearbox casing [4]. These loading conditions, while critical for component dimensioning, remain largely unaddressed by conventional test methodologies.

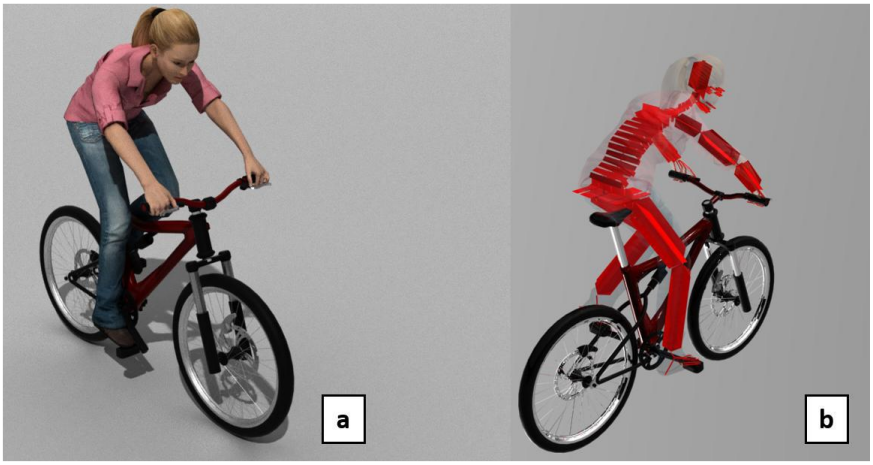

Figure 1. Anthropomorphic rider model transferred to the biomechanical pedelec test bench at Aalen University. With a: simulation model of the virtual rider and b: anthropomorphic skeleton model of the rider, based on findings of Prof. Feldmann [17], [18], published in [5].

The motivation for developing an advanced biomechanical test bench arises from documented field failures that cannot be reproduced using traditional testing approaches. Micro-cracks, surface pitting, and progressive wear patterns observed in field-returned drive units often differ fundamentally from damage patterns generated in laboratory environments. This discrepancy suggests that conventional test protocols inadequately represent the true loading spectrum experienced during real-world operation. Moreover, the expanding application range of pedelecs—from urban commuter vehicles and corporate fleet bicycles to cargo bikes for delivery services and high-performance mountain bikes demands differentiated testing protocols that account for application-specific load collectives.

The present work introduces a novel control concept for a biomechanical pedelec test bench (HiL[1]-Testbench) developed at Aalen University of Applied Sciences in collaboration with *daum electronics GmbH*. The fundamental innovation lies in the integration of a digital twin representing both the rider's biomechanical behavior and the environmental conditions, coupled through a real-time Hardware-in-the-Loop (HiL) architecture. Rather than prescribing fixed speed or torque trajectories as in conventional approaches, the test bench allows the resulting vehicle dynamics to emerge from the interaction between the load-collectives of the simulated rider model, the physical test specimen, and the virtual environment model. This paradigm shift enables the reproduction of realistic damage patterns that were previously unattainable under laboratory conditions.

The control architecture comprises three interconnected subsystems: (1) the biomechanical rider model, which generates physiologically realistic pedal torque profiles including the characteristic negative torque phases during leg recovery, phase-shifted left-right actuation, and situation-dependent variations such as standing pedaling with associated radial loading; (2) the environmental simulation model, which computes speed-dependent road resistance, gradient

[1] Hardware-in-the-Loop

effects, and inertial loads based on recorded route data; and (3) the real-time data acquisition and correlation system, which synchronizes actuator commands with sensor feedback at sampling rates up to 10 kHz while logging comprehensive test data for post-processing analysis.

This paper is structured as follows: Section 2 reviews related work on bicycle drivetrain testing and biomechanical modeling of cycling. Section 3 presents the mechanical design of the test bench with emphasis on the actuation systems for pedal drive and load simulation. Section 4 details the control concept, including the mathematical formulation of the rider model, the environmental simulation, and the HiL integration architecture. Section 5 describes the experimental validation through endurance tests covering over 20,000 km equivalent distance. Section 6 discusses the results, comparing observed damage patterns with field data and conventional test outcomes. Finally, Section 7 concludes with perspectives on future extensions including AI-based predictive maintenance algorithms.

2. STATE OF THE ART

2.1 Pedelec drivetrain architecture and loading characteristics

Pedelec drivetrains are fundamentally hybrid systems that combine human pedal power with electric motor assistance. The dominant configuration employs a mid-drive motor integrated at the bottom bracket, where both power sources merge on a common output shaft driving the chainring [5]. This architecture requires the gearbox to transmit the superimposed torques from rider and motor while accommodating the cyclic nature of pedal loading. The legal framework significantly influences drivetrain specifications. Standard pedelecs are limited to 250 W nominal motor power with assistance ceasing at $25\ km/h$, while S-Pedelecs permit up to four times the instantaneous pedal power with a $45\ km/h$ cutoff [6]. Peak torques at the chainring can reach 100 Nm during aggressive riding, substantially exceeding loads encountered in conventional bicycles. These requirements have driven the development of compact planetary gear systems with transmission ratios typically around $i = 50$, necessitating precise gear geometry and robust bearing arrangements. The cyclic pedal torque presents a distinctive loading pattern. Biomechanical studies by Petzke [7] characterized the torque contribution of each leg over a complete crank revolution. The effective torque exhibits a quasi-sinusoidal profile with maximum values occurring near 100° crank angle during the power phase. Notably, negative torque contributions arise between 195° and 360° as the recovering leg must be lifted against gravity, creating a characteristic torque valley. The resultant chainring torque from both legs shows two peaks per revolution, phase-shifted by approximately 180°.

2.2 Conventional Drivetrain Testing Approaches

Established methodologies for drivetrain durability testing predominantly rely on constant or stepped load profiles. Standard protocols specify discrete torque-speed combinations maintained for defined durations, with the test specimen cycled through multiple operating points [8]. While such approaches efficiently accumulate fatigue cycles, they inadequately represent the transient loading inherent to cycling. Block loading programs represent an advancement by incorporating variable amplitude fatigue. Typical implementations define load collectives based on statistical analysis of field measurements, applying counted cycles at different stress levels according to damage accumulation hypotheses [9]. However, block loading fundamentally decouples the temporal correlation between load events, eliminating the sequential dependencies characteristic of real riding scenarios such as acceleration-deceleration sequences or terrain transitions.

Roller-based test rigs enabling complete bicycle testing have been implemented for frame and component qualification [10]. These systems typically employ servo-hydraulic actuators applying vertical and horizontal forces to the saddle and handlebars while the bicycle rolls on drums. Although capturing some aspects of structural loading, such configurations generally lack the capability to replicate realistic pedal input, instead using constant-torque motor drives at the crank.

2.3 Biomechanics of Cycling

The biomechanical analysis of pedaling reveals substantial complexity beyond simple rotational motion. The human leg functions as a multi-segment kinematic chain comprising hip, knee, and ankle joints, each contributing to pedal force generation through coordinated muscle activation [11]. The resulting pedal force vector varies continuously in both magnitude and direction throughout the crank cycle. Force decomposition distinguishes tangential components contributing to propulsion from radial components that load the bearings without generating useful work.

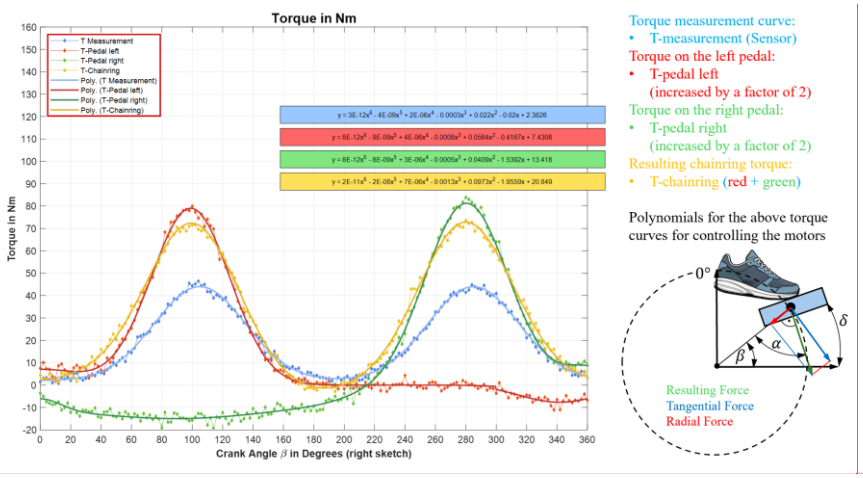

Figure 2. Pedal torque profiles over one crank revolution showing left pedal (red), right pedal (green), and resultant chainring torque (yellow). Polynomial approximations for motor control shown as smoothed curves (adapted Model), first model originally developed by Prof. Körner and measurements established at the e-Bike Testbench (HSAA).

Skilled cyclists optimize pedaling technique to maximize the tangential fraction, yet significant radial forces persist particularly during high-power output [12]. The force application point and direction are characterized by the crank angle β, pedal angle δ, and the resultant force angle $\alpha = \beta + \delta$, as illustrated in Fig. 2. Standing pedaling ('Wiegeschritt') introduces additional loading modes absent during seated cycling. The rider's body mass shifts laterally with each pedal stroke, generating alternating moments about the bicycle's longitudinal axis. This motion induces substantial lateral forces at the bottom bracket, causing measurable housing deformation. Körner et al. [4] documented deflections up to 0.45 mm at pedelec gearbox housings during standing pedaling, sufficient to alter gear mesh conditions and contact patterns.

2.3 Hardware-in-the-Loop testing

Hardware-in-the-Loop methodologies have achieved widespread adoption in automotive powertrain development, enabling the integration of physical components with virtual vehicle models [13]. The fundamental principle substitutes selected system components with real-time simulations while retaining hardware elements of interest. This approach offers advantages for testing electronic control units, validating software functionality, and conducting accelerated durability programs under controlled conditions. Application to two-wheeled vehicles remains comparatively limited. Sivert et al. [14] developed an electrical bicycle platform for educational purposes incorporating regenerative braking simulation. Commercial dynamometer systems for e-bike motor characterization exist but typically emphasize steady-state efficiency mapping rather

Kommentiert [MW1]: Der zweite Teil des blauen Sinuses muss negativ sein, da das Pedal das Bein des Fahrers nach oben drücken muss. Die Messung bezieht sich auf ein Pedal

than transient durability assessment. The integration of rider biomechanics into HiL test benches represents largely unexplored territory. Existing cycling simulators developed for sports science applications focus on metabolic response and performance optimization rather than drivetrain loading [15]. The translation of anthropometric models into actuator commands for hardware testing requires addressing real-time constraints, force bandwidth limitations, and the coupling between simulated rider behavior and physical system response.

2.4 Hardware-in-the-Loop testing

The reviewed literature reveals a significant gap between biomechanical understanding of cycling and practical drivetrain testing methodologies. While the complex, time-varying nature of pedal loading is well documented, this knowledge has not been systematically incorporated into durability test protocols. Conventional approaches implicitly assume that simplified load representations adequately capture fatigue-relevant stress states an assumption contradicted by discrepancies between laboratory and field failure modes. The present work addresses this gap through a control concept that explicitly incorporates biomechanical rider modeling into Hardware-in-the-Loop drivetrain testing. The key differentiator from prior art lies in the emergent nature of the resulting load spectrum: rather than prescribing predetermined torque trajectories, the test bench allows realistic loading to arise from the dynamic interaction between simulated rider, physical specimen, and virtual environment. This approach preserves the temporal correlations and load sequence dependencies inherent to actual cycling while enabling reproducible, accelerated testing under laboratory conditions.

3. TEST BENCH DESIGN AND MECHANICAL SETUP

3.1 System Overview

The biomechanical pedelec test bench was developed to enable realistic durability testing by replicating the complex loading conditions encountered during actual cycling. Fig. 3 presents an isometric view of the complete system, identifying the principal components. The test bench integrates three primary functional subsystems: the pedal drive system simulating rider input, the load simulation system representing road resistance and vehicle inertia, and the instrumentation system for real-time data acquisition and safety monitoring.

3.2 Pedal Drive System

The pedal drive system constitutes the core innovation enabling biomechanical load application. Two synchronous servo motors [d.1, d.2] independently actuate the left and right pedal cranks, permitting phase-shifted torque profiles characteristic of human pedaling. The motors are SEW synchronous servo units rated for peak torques of 665 Nm with a gear reduction ratio of 23.44:1, providing sufficient bandwidth to reproduce the dynamic torque variations occurring during realistic pedaling at cadences up to 120 rpm. Power transmission from motors to pedal cranks employs a cardan joint arrangement [j] mounted on a movable servomotor platform. This configuration accommodates the lateral displacement inherent to standing pedaling simulation while maintaining precise angular synchronization. The cardan joints introduce minimal backlash and permit controlled misalignment without inducing parasitic loads on the crank bearings.

Non-contact torque measuring shafts [f.1, f.2] manufactured by Mayr are positioned between each motor output and the corresponding pedal crank. These precision transducers provide real-time torque feedback with measurement uncertainty below 0.1% of full scale, enabling closed-loop torque control and simultaneous data logging for post-test analysis. The contactless operating principle eliminates wear-related drift, ensuring measurement stability throughout extended durability campaigns.

3.3 Load Simulation System

The output-side load simulation replicates the resistance forces acting on the bicycle during road operation. A SEW geared motor [c] drives the rear wheel contact roller, functioning as a

controllable brake or, when required, as a drive source for regenerative scenarios. The motor specification includes a nominal torque of 425 Nm enabling simulation of steep gradients, headwind conditions, and aggressive deceleration events.

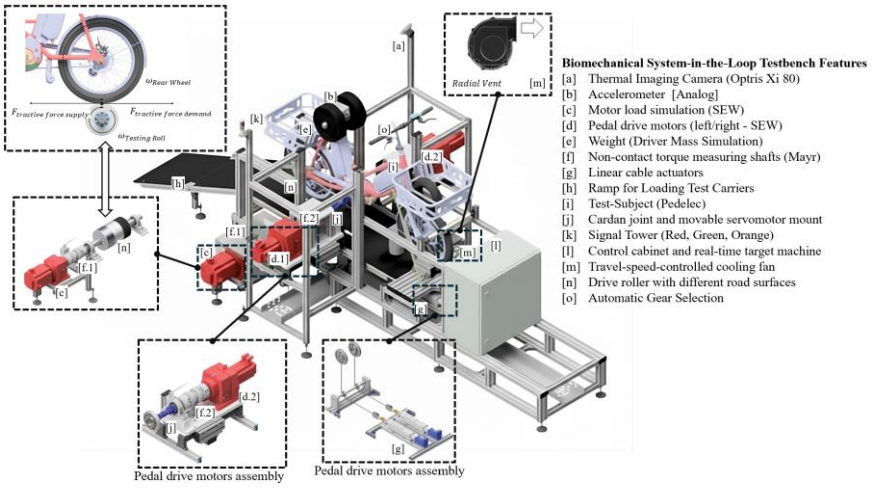

Figure 3. Isometric view of the biomechanical pedelec test bench identifying principal components: [a] thermal imaging camera, [b] accelerometer, [c] load simulation motor, [d.1/d.2] pedal drive motors, [e] rider mass simulation, [f.1/f.2] torque measuring shafts, [g] linear cable actuators, [h] loading ramp, [i] test specimen, [j] cardan joint assembly, [k] signal tower, [l] control cabinet, [m] cooling fan, [n] testing roll, [o] automatic gear change mechanism.

The roller assembly incorporates interchangeable surface elements permitting simulation of different road textures. Smooth cylindrical sections represent asphalt surfaces, while profiled attachments can replicate cobblestones or off-road conditions, generating characteristic vibration signatures transmitted through the drivetrain. A horizontal displacement mechanism allows transitioning between surface types during test sequences without interrupting operation.

Rotational inertia simulation presents particular challenges for bicycle testing, as the relatively low vehicle mass results in rapid acceleration dynamics. The test bench addresses this through a combination of physical flywheel elements and electronic inertia emulation. Stacked steel discs mounted on the roller shaft provide base inertia, while the motor controller superimposes calculated inertial torques based on the virtual vehicle model, achieving accurate representation of acceleration and braking transients.

3.4 Radial Load Actuation

Standing pedaling introduces significant lateral forces at the bottom bracket as the rider's weight shifts between pedals. Linear cable actuators [g] replicate these radial loads by applying alternating vertical forces to the crank bearings synchronized with pedal position. The actuators connect to the bottom bracket region via cable guides, pulling downward on each side in phase with the corresponding power stroke. The actuation system generates forces representative of a 75 kg rider performing aggressive standing pedaling, with peak radial loads reaching approximately 500 N per side. Force magnitude and phasing are programmable parameters within the control system, enabling investigation of different rider weights and pedaling styles. This capability addresses the housing deformation effects identified by Körner et al. [4] as significant factors in gear contact pattern evolution.

3.5 Test Specimen Integration

The test specimen, a complete pedelec, mounts within the test bench frame using adjustable pillar supports with spring tensioners maintaining tire contact with the rollers., Fig [3] and Fig[4] Accommodation of different wheelbase dimensions is achieved through variable roller spacing [see Fig. 2, green arrows in reference documentation], while lateral guides prevent uncontrolled lateral drift during dynamic testing.

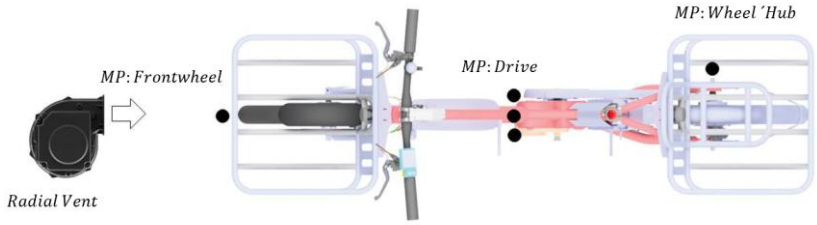

Figure 4. Schmatic experimental setup of the cargo pedelec

For the present investigation, the test specimen [i] comprised a cargo pedelec equipped with a central drive motor and Shimano Nexus 8-speed internal gear hub. The original battery was substituted with a laboratory power supply (Elektro-Automatik PSI-8080-60 T) providing stable voltage and enabling precise measurement of electrical power consumption. Weight simulation [e] replicates rider mass through calibrated masses mounted at the saddle position, totaling approximately 20 kg for the baseline configuration. The test

3.6 Instrumentation and Safety Systems

Comprehensive instrumentation enables both control feedback and scientific data acquisition. Table 1 summarizes the principal measured quantities and sensor specifications. The data acquisition system records 42 parameters at 100 Hz sampling rate, with burst capability to 10 kHz for transient event capture.

Table 1. Principal instrumentation specifications

Parameter	Sensor Type	Range	Location
Pedal torque L/R	Mayr non-contact	0–100 Nm	Motor output shafts [f]
Roller torque	Mayr non-contact	0–500 Nm	Load motor shaft
Pedal position L/R	Integrated encoder	0–360°	Servo motors [d]
Cadence	CAN bus	0–150 rpm	Pedelec internal
Drive temperature	CAN bus	–20–120 °C	Pedelec internal
Frame acceleration	3-axis MEMS [b]	±30 g	Bottom bracket region
Surface temperature	Thermal camera [a]	0–250 °C	Motor housing

A thermal imaging camera (Optris Xi 80) [a] provides non-contact temperature monitoring of the drive unit housing, enabling detection of abnormal heating indicative of bearing degradation or lubricant breakdown. The camera's 80 × 80 pixel resolution and 50 Hz frame rate permit identification of localized hot spots with spatial resolution adequate for component-level diagnosis. The accelerometer system [b] serves dual purposes: characterization of vibration signatures for correlation with road surface simulation, and safety monitoring for collision detection. Acceleration thresholds trigger immediate motor shutdown if exceeded, preventing

damage from mechanical failures or specimen ejection. A signal tower [k] with red, green, and orange indicators provides visual status indication visible throughout the laboratory. The control cabinet [l] houses the real-time target machine, motor drives, and safety relay systems. Access interlocks ensure that motor power is disabled whenever the safety enclosure is breached.

3.7 Cooling and Environmental Control

Extended durability testing generates substantial heat within the drive unit, potentially influencing failure mechanisms and accelerating lubricant degradation. A speed-controlled cooling fan directs airflow over the motor housing, with fan speed modulated either proportionally to simulated vehicle speed (replicating headwind cooling) or thermostatically based on measured housing temperature, compare Fig. 3 [m]. Target temperature setpoints are programmable, enabling investigation of thermal effects on component durability.

The test facility maintains ambient temperature within 18–25 °C through laboratory climate control, eliminating seasonal variations that could confound long-term test comparisons. Humidity is not actively controlled but is logged for reference.

4. Control Concept and Algorithm

4.1 Control Architecture Overview

The control architecture integrates three interconnected domains: the biomechanical rider model generating pedal torque commands, the environment model computing road load resistance, and the Hardware-in-the-Loop (HiL) platform coordinating real-time execution. Fig. 5 illustrates the system architecture, highlighting the bidirectional data flow between the virtual rider, the physical test specimen, and the simulated environment.

The fundamental control philosophy distinguishes this test bench from conventional dynamometers. Rather than prescribing fixed speed or position trajectories, the system operates in torque-control mode throughout. The pedal actuators apply torques derived from the biomechanical model, the load motor applies resistance torques computed from the environment simulation, and the resulting vehicle dynamics emerge from the physical interaction. This approach preserves the natural coupling between rider effort, motor assistance, and vehicle response characteristic of actual cycling.

The real-time target machine serves as the central coordination platform, executing the control algorithms at 1 kHz sampling rate while managing communication with peripheral systems. Motor drive commands are transmitted via EtherCAT to the SEW servo controllers, pedelec internal data is acquired through CAN bus interface, and analog sensor signals are digitized through dedicated I/O modules. A separate HMI interface running on an external PC provides operator visualization and parameter adjustment without compromising real-time determinism.

4.2 Biomechanical Pedal Torque Model

The pedal torque model replicates the characteristic loading pattern produced by human legs during cycling. Based on biomechanical measurements by Petzke [7] and validated through instrumented test rides by Prof. Körner (HSAA), the model generates separate torque profiles for left and right pedals as functions of crank angle. The instantaneous torque at each pedal comprises a positive propulsion component during the power phase and a negative component during leg recovery. For the left pedal, the torque profile is expressed as:

$$T_{pedal}, L(\beta) = T_{max} \cdot f_{prop}(\beta) + T_{neg} \cdot f_{rec(\beta)} \quad (1.1)$$

where β denotes the crank angle in degrees, T_{max} is the peak propulsion torque, T_{neg} is the recovery phase torque magnitude, and f_{prop} and f_{rec} are normalized shape functions.

The propulsion shape function captures the quasi-sinusoidal torque rise during the power stroke:

$$f_{prop}(\beta) = e^{\left(-\frac{(\beta-\beta_{peak})^2}{2\sigma_{prop}^2}\right)} \cdot [1 - S(\beta, \beta_{trans}, k_{trans})]$$

where $\beta_{peak} \approx 100°$ defines the crank angle of maximum torque, σ_{prop} controls the width of the power phase, and $S(\beta, \beta_{trans}, k_{trans})$ is a sigmoid transition function:

$$S(\beta, \beta_{trans}, k) = \frac{1}{1+e^{\left(-k(\beta-\beta_{trans})\right)}} \tag{1.2}$$

The recovery phase function models the negative torque arising from lifting the leg mass against gravity:

$$f_{rec}(\beta) = -\sin^2\left(\frac{\pi \cdot \beta}{180}\right) - \cdot [1 - S(\beta, 180°, 0.1)] \tag{1.3}$$

This formulation produces negative torque contributions in the range $195° < \beta < 360°$, consistent with measured pedaling biomechanics.

The right pedal torque follows an identical functional form with $180°$ phase offset:

$$T_{pedal,R}(\beta) = T_{pedal,L}(\beta - 180°) \tag{1.4}$$

The resulting chainring torque represents the superposition of both pedal contributions:

$$T_{chainring}(\beta) = T_{pedal,L}(\beta) + T_{pedal,R}(\beta) \tag{1.5}$$

This summation produces the characteristic dual-peak profile with maxima near $100°$ and $280°$ crank angle, as illustrated in Fig. 2.

4.3 Load-Dependent Torque Scaling

The peak pedal torque T_{max} varies dynamically based on the simulated riding situation. A motivation model scales the baseline torque according to the deviation between actual and desired velocity:

$$T_{max}(t) = T_{base} \cdot \left[1 + k_v \cdot \tanh\left(\frac{v_{target} - v_{actual}}{\Delta v}\right)\right] \tag{1.6}$$

where T_{base} is the nominal pedal torque for steady-state cruising, k_v is the velocity error gain, and Δv defines the velocity deviation scaling. This formulation causes the virtual rider to increase effort when below target speed (e.g., climbing) and reduce effort when exceeding it (e.g., descending).

4.4 Power Balance and Motor Assistance

The pedelec drive system operates as a hybrid powertrain where rider and motor contributions sum at the chainring. The control system maintains a target combined power output:

$$P_{total} = P_{pedal} + P_{motor} = 500\ W \tag{1.7}$$

The pedal power derives from the applied torque and cadence:

$$P_{pedal} = T_{chainring} \cdot \omega_{pedal} = T_{chainring} \cdot \frac{2\pi \cdot n_{cadence}}{60} \tag{1.8}$$

where $n_{cadence}$ is the pedaling cadence in rpm.

The motor assistance is governed by the pedelec's internal control unit, which modulates output torque proportionally to measured pedal torque according to the selected support mode. The support factor F_u determines the motor contribution:

$$P_{motor} = P_{pedal} \cdot (F_u - 1) \tag{1.9}$$

where typical support factors are:

- ECO mode: $F_u = 0.50$ (50% $assistance$)

- TOUR mode: $F_u = 1.20$ $(120\%\ assistance)$
- SPORT mode:$F_u = 2.10$ $(210\%\ assistance)$
- TURBO mode: $F_u = 3.00$ $(300\%\ assistance)$

The motor assistance is communicated and controlled via CAN bus through the real-time target machine. Above the regulation threshold velocity (typically 18 km/h), the support factor progressively decreases according to:

$$F_{u(v)} = F_{u,nom} \cdot \left[1 - \frac{v - v_{threshold}}{v_{max} - v_{threshold}}\right] \quad for\ v > v_{threshold} \tag{1.10}$$

reaching zero assistance at $v_{max} = 25\frac{km}{h}$ for standard pedelecs.

4.5 Environment and Road Load Model

The load motor applies resistance torque computed from the virtual environment model. The total road load force comprises rolling resistance, aerodynamic drag, gradient resistance, and acceleration forces:

$$F_{road} = F_{roll} + F_{aero} + F_{grade} + F_{accel} \tag{1.11}$$

Individual components are computed as:

$$F_{roll} = \mu_{roll} \cdot m_{total} \cdot g \cdot cos(\alpha_{grade}) \tag{1.12}$$

$$F_{aero} = \frac{2}{1} \cdot \rho_{air} \cdot C_d \cdot A \cdot v^2 \tag{1.13}$$

$$F_{grade} = m_{total} \cdot g \cdot sin(\alpha_{grade}) \tag{1.14}$$

$$F_{accel} = m_{total} \cdot \frac{dt}{dv} \tag{1.15}$$

where μ_{roll} is the rolling resistance coefficient (typically $0.006 - 0.010$ for bicycle tires), m_{total} is the combined mass of bicycle, rider, and cargo, α_{grade} is the road gradient angle, ρ_{air} is air density, C_d is the drag coefficient, and A is the frontal area.

The required load torque at the roller is:

$$T_{load} = F_{road} \cdot r_{wheel} \cdot \frac{1}{i_{drivetrain}} \tag{1.16}$$

where r_{wheel} is the wheel radius and $i_{drivetrain}$ is the overall transmission ratio from chainring to wheel.

Route profiles recorded during test drives provide time-series data for gradient, target velocity, and surface type, enabling reproduction of specific routes under laboratory conditions.

4.6 Real-Time Implementation

The control algorithms are implemented in CODESYS, an IEC 61131-3 compliant development environment that generates executable code for the SEW MOVI-C controller platform. The software architecture comprises cyclic tasks executing at defined intervals:

Table 2. Control task configuration

Task	Cycle Time	Function
Motion Control	1 ms	Torque command generation, servo communication
Data Acquisition	10 ms	Sensor sampling, CAN bus polling
Supervision	10 ms	Safety monitoring, state machine
Logging	10 ms	Data recording to file system

The motion control task computes instantaneous pedal torques based on current crank angle, retrieved from motor encoder feedback, and transmits torque setpoints to the servo drives via EtherCAT. The SEW drives operate in torque control mode with current loop bandwidth exceeding 1 kHz, ensuring accurate reproduction of the commanded torque profiles.

Data from the real-time target machine are logged continuously and forwarded to the SEW controller for synchronized storage. Each logged dataset contains up to 1,600,000 samples at 100 Hz, corresponding to approximately 16,000 seconds of test duration. Extended test campaigns generate multiple sequential files that are concatenated during post-processing.

4.7 'Wiegeschritt' (Standing Pedaling) Mode

Standing pedaling introduces additional loading modes requiring coordinated actuation of the radial force actuators. When 'Wiegeschritt' mode is activated, the cable actuators apply alternating vertical forces synchronized with pedal position:

$$F_{radial,L}(\beta) = F_{(rad,\max)} \cdot \sin^2\left(\frac{\pi \cdot \beta}{180}\right) \cdot H(\beta_{start} < \beta < \beta_{end}) \tag{1.17}$$

$$F_{(radial,R)(\beta)} = F_{(radial,L)(\beta - 180°)} \tag{1.18}$$

where $F_{rad,max}$ is the peak radial force (approximately $500\ N$ for a $75\ kg$ rider), and $H(\dots)$ is a window function limiting application to the power phase. The pedal torque magnitudes are simultaneously increased by a configurable multiplier (typically $1.5 - 2.0\times$) reflecting the enhanced force application possible during standing pedaling.

4.8 Automatic Gear Selection

An optional automatic gear change mechanism replicates rider shifting behavior, compare Fig. 3 [o]. The algorithm monitors cadence and selects gear ratios to maintain cadence within a target band:

$$if\ n_{cadence} > n_{max}: shift\ up$$

$$if\ n_{cadence} < n_{min}: shift\ down$$

Gear changes are executed through a servo-actuated cable pull system with configurable shift delay to prevent hunting. The gear state is logged as part of the test data for correlation with observed wear patterns.

---

5. Experimental Validation

5.1 Test Campaign Overview

The biomechanical control concept was validated through an extensive endurance test campaign conducted between February and July 2021. The test specimen was a cargo pedelec equipped with a central drive unit (serial number 00944120) and Shimano Nexus 8-speed internal gear hub. Testing accumulated a total distance of 20,007 km over 5,612,942 seconds of operation, representing approximately 1,560 hours of continuous drivetrain loading[2].

The test protocol implemented a stepped load collective (5 Stages) derived from field measurements, performed under realistic cargo-bike load conditions. Each test cycle comprised five phases executed over 25 minutes total duration:

[2] Generic sample values

Table 3. Example of typical test cycle load collective[3]

Phase	Duration	Cadence	P_pedal	P_motor	P_total	T_chainring
1	5 min	60 rpm	250 W	250 W	500 W	47.75 Nm
2	5 min	80 rpm	301 W	250 W	551 W	52.64 Nm
3	5 min	100 rpm	284 W	250 W	534 W	51.01 Nm
4	5 min	50 rpm	227 W	250 W	477 W	45.58 Nm
5	5 min	0 rpm	0 W	0 W	0 W	0 Nm

The cooling phase between cycles permitted thermal relaxation of the drive unit, with forced air cooling maintaining housing temperature below 55°C. This protocol accumulated approximately 300 km equivalent distance per 24-hour period during continuous autonomous operation.

5.2 Control Loop Performance

Fig. 5 presents the closed-loop control performance during a representative test cycle. The upper plots show commanded versus measured torque for left and right pedal motors, demonstrating tracking accuracy within ±2% across the operating range. The biomechanical torque profile is clearly visible, with the characteristic dual-peak pattern and negative recovery phase faithfully reproduced.

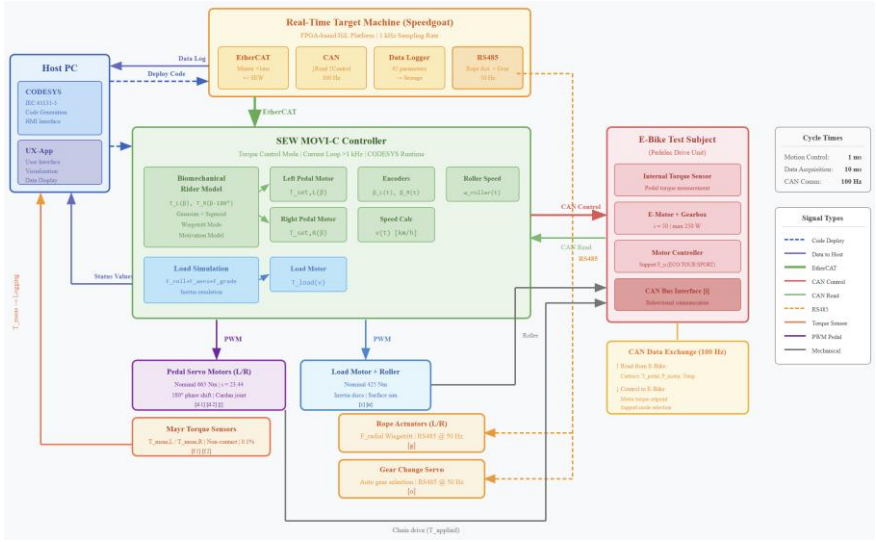

Figure 5. Control loop architecture showing signal flow between biomechanical rider model, real-time HiL platform, servo drives, test specimen, and load simulation. Torque-controlled actuation enables emergent vehicle dynamics.

The control loop implements the following structure:

$$T_{cmd}(t) = T_{model}\big(\beta(t)\big) + K_p \cdot e_T(t) + K_i \cdot \int e_T(t)dt \tag{1.19}$$

where T_{model} is the feedforward torque from the biomechanical model, $e_T = T_{cmd} - T_{meas}$ is the torque tracking error, and K_p, K_i are proportional and integral gains. The feedforward term

[3] Table contains generic values due to compliance reasons

dominates during normal operation, with the feedback terms compensating for friction variations and dynamic effects.

The load motor control maintains the computed road resistance:

$$T_{load,cmd}(t) = T_{road}(v(t), \alpha(t)) + J_{equiv} \cdot \frac{d\omega}{dt} \quad (1.20)$$

where the second term provides electronic inertia emulation. Measured roller speed serves as feedback for velocity-dependent resistance calculation.

CAN bus communication with the pedelec drive unit operates at 100 Hz, retrieving internal sensor data including pedal torque (as measured by the drive unit's own sensor), motor temperature, cadence, and instantaneous power. This data enables validation of the external torque application against the drive unit's internal perception, confirming that the simulated loading appears authentic to the motor controller.

5.3 Accumulated Test Distance and Operating Statistics

The test campaign accumulated a total distance of 20,007 km as recorded by the drive unit's internal odometer, with total operating time of 5,613,000 seconds (approximately 1,559 hours). Table 4 summarizes key operating statistics:

Table 4. Endurance test statistics

Parameter	Value
Total distance	20,007 km
Total operating time	1,559 hours
Average speed	12.8 km/h
Average cadence	97 rpm
Average pedal torque	24.3 Nm
Peak pedal torque	52.6 Nm
Average motor temperature	38°C
Maximum motor temperature	54°C

Data logging generated datasets totaling over 150 MB per 300 km segment, with 42 parameters recorded at 100 Hz sampling rate. Post-processing analysis confirmed consistent load application throughout the campaign, with less than 3% variation in cycle-averaged torque values.

5.4 Observed Failure Modes

This chapter contains generic testing results of a cargo pedelec prototype. The extended test campaign is producing several component failures providing insight into realistic damage mechanisms. Table 5 chronologically documents observed failures:

Table 5. Typical example of documented failures during endurance testing[4]

Distance [km]	Date	Component	Failure Mode	Root Cause
1,822	16.02.21	Hub gear	Slipping	Overheating (no cooling)
2,623	20.02.21	Chain guard	Fracture	Chain wear, housing stress
7,908	13.04.21	Chain	Fracture	Wear accumulation
8,104	14.04.21	Rear hub bearing	Pitting	Overload, chain tension
15,660	31.05.21	Chain	Fracture	Wear accumulation
17,604	11.06.21	Rear hub bearing	Pitting	Repeated overload
17,939	15.06.21	Chain tensioner	Tooth fracture	Misalignment, tension
19,800	02.07.21	Chain tensioner	Tooth fracture	Accumulated fatigue

[4] Table contains generic values due to compliance reasons

Significantly, the central drive unit itself the primary test object exhibited no functional failures throughout the 20,000 km campaign, demonstrating robust design margins for the tested load collective. Post-test inspection revealed minor wear patterns consistent with normal operation but no incipient damage threatening continued function.

5.6 Human-Machine Interface

The test bench operation is controlled through a MATLAB-based graphical user interface (GUI) developed at Hochschule Aalen, designated "eBike Simulator" (Fig. 6). The interface provides comprehensive control and monitoring capabilities organized across four functional tabs: eBike-Control, Data_Evaluation_1, Data_Evaluation_2, and Instructions.

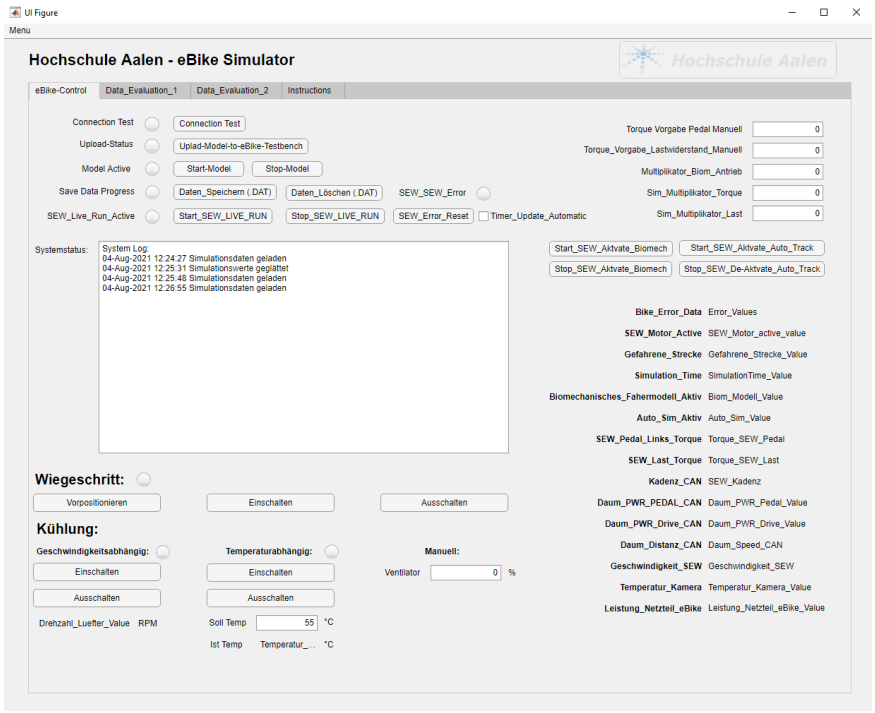

Figure 6. MATLAB-based graphical user interface (GUI) for test bench operation. The eBike-Control tab provides connection management, drive control, manual parameter input, biomechanical model activation, real-time status monitoring, and cooling system control.

Figure 6. MATLAB-based graphical user interface (GUI) for test bench operation. The eBike-Control tab provides connection management, drive control, manual parameter input, biomechanical model activation, real-time status monitoring, and cooling system control.

The primary control tab (eBike-Control) is structured into distinct functional areas. The connection and model management section in the upper left establishes communication with the real-time target machine through a sequential initialization procedure. The "Connection Test" button verifies the link between Host PC and Speedgoat target. Upon successful connection, "Upload-Model-to-eBike-Testbench" transfers the compiled control model to the real-time system. "Start-Model" and "Stop-Model" buttons activate and deactivate the control algorithms,

with status indicators adjacent to each button providing visual feedback on connection state and model execution status.
Data management functions handle measurement data storage and deletion on the target system through dedicated buttons. The SEW_Error indicator and reset button provide fault management for the servo drive system, while an automatic timer function enables periodic status polling. Drive control buttons directly control the servo motor activation state, with a dedicated indicator confirming when the drives are energized and operational.
Manual parameter input fields in the upper right enable real-time adjustment of critical test parameters including manual pedal torque setpoint, manual load resistance setpoint, scaling factor for the biomechanical drive model, and real-time multipliers for torque and load. These parameters allow operators to fine-tune test conditions without interrupting ongoing experiments.
The biomechanical model control section provides dedicated buttons to activate the biomechanical rider simulation and the automatic test track execution. These functions enable switching between manual operation and automated test cycle execution, supporting both exploratory testing and standardized endurance campaigns.
A comprehensive system status display panel shows real-time values for all critical parameters: E-Bike system fault codes, servo drive activation state, accumulated test distance, current test duration, rider model activation status, automatic simulation mode status, left pedal torque command, load motor torque command, cadence from the E-Bike CAN bus, pedal and motor power readings, distance from the E-Bike odometer, calculated velocity, thermal camera temperature reading, and power supply consumption. A timestamped event log records all significant system events including model uploads, parameter changes, and error conditions.
Standing pedaling simulation (Wiegeschritt) is managed through three control buttons: "Vorpositionieren" to pre-position the actuators, "Einschalten" to activate, and "Ausschalten" to deactivate. This enables controlled investigation of radial loading effects on the drivetrain under representative out-of-saddle cycling conditions.

The thermal management interface at the bottom of the control panel provides three operating modes: speed-dependent control where fan speed is proportional to simulated vehicle velocity, temperature-dependent control with a configurable setpoint (typically 55°C), and manual control for direct fan speed adjustment via percentage input. Current temperature and fan speed values are continuously displayed for monitoring.
The MATLAB GUI communicates with the Speedgoat real-time target via Ethernet using UDP/TCP protocols and provides the operator interface for test configuration, execution monitoring, and emergency intervention. All parameter changes are transmitted to the real-time system without interrupting ongoing test execution, enabling dynamic adjustment of test conditions during long-duration endurance campaigns.

5.7 Load Collective Definition

The endurance test protocol employs a five-stage stepped load collective derived from representative field usage profiles (Fig. 7). Each test cycle comprises sequential load stages of equal duration, providing systematic variation in power distribution between rider and motor assistance while maintaining the biomechanical torque profile characteristics.
Figure 7. Stepped load collective showing power distribution across five stages. Blue bars indicate electric motor power at chainring, gray bars represent pedal power contribution, orange bars show total combined power, and yellow bars denote cadence. Stage 5 serves as thermal recovery phase with zero load.
Stage 1 establishes the baseline condition at 500 W total power with equal contribution from rider (250 W) and motor (250 W), representing balanced assistance typical of moderate touring conditions. The cadence is maintained at approximately 95 rpm throughout powered stages.
Stage 2 increases total power to 551 W by elevating pedal power to 301 W while motor power remains at 250 W. This configuration simulates reduced assistance scenarios where the rider

compensates for terrain changes or battery conservation modes, resulting in an effective support factor of 83%.

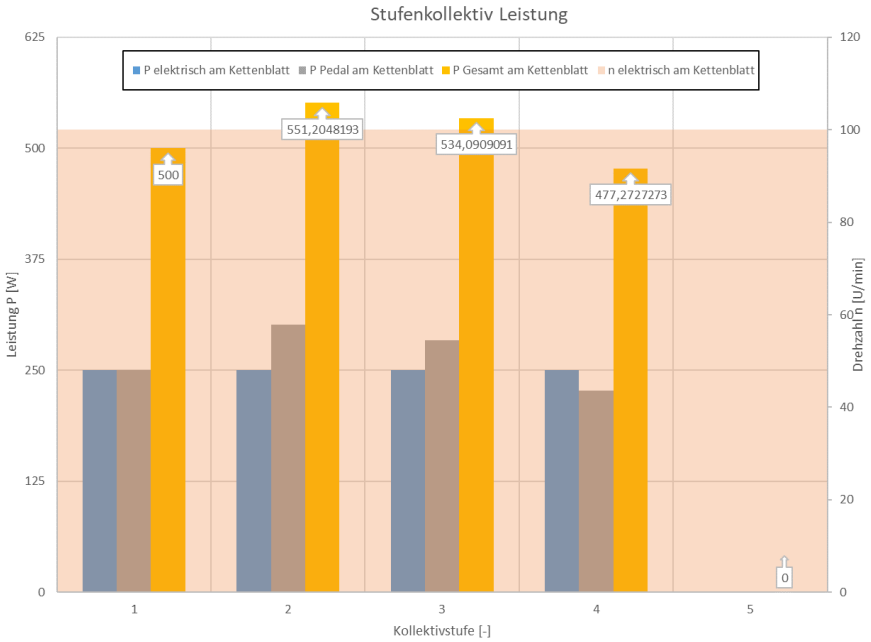

Figure 7. Load collective chainring

Stage 3 operates at 534 W total power with 284 W pedal contribution and 250 W motor assistance, corresponding to an 88% support factor. This intermediate load level represents typical urban commuting conditions with moderate assistance.
Stage 4 reduces total power to 477 W through decreased pedal input (227 W) while maintaining 250 W motor power, yielding a 110% support factor. This configuration simulates high-assistance modes where motor contribution exceeds rider effort, characteristic of SPORT or TURBO assistance settings.
Stage 5 constitutes a zero-load cooling phase where both pedal and motor power are suspended. This thermal recovery period allows the drive unit to dissipate accumulated heat, preventing thermal runaway during continuous operation. The cooling phase duration is adjusted based on measured housing temperature to maintain operation below the 55°C threshold.
The load collective cycles continuously during autonomous endurance testing, with each complete cycle lasting 25 minutes (5 minutes per stage). This protocol subjects the drivetrain to varying torque amplitudes and power distributions while maintaining consistent biomechanical loading characteristics, ensuring representative fatigue accumulation across all operating conditions encountered in field service.

3. CONCLUSIONS

This paper presented a biomechanical Hardware-in-the-Loop control concept for pedelec drivetrain testing that integrates digital twin models of rider and environment with physical test specimens. The key innovation lies in torque-controlled actuation generating emergent vehicle dynamics rather than prescribed motion trajectories, preserving the natural coupling between rider

effort, motor assistance, and road load characteristic of actual cycling. The control architecture implements biomechanical pedal torque profiles with physiologically realistic phase relationships using Gaussian-Sigmoid transition functions and negative recovery torque. Load-dependent torque scaling through a virtual rider motivation model adapts effort based on velocity deviation, while power-balanced operation maintains 500 W combined output with authentic support factor emulation. Real-time coordination through CODESYS on SEW MOVI-C platforms achieves 1 kHz motion control, with CAN bus integration enabling bidirectional communication with the pedelec drive unit. RS485-controlled auxiliary systems provide Wiegeschritt simulation and automatic gear selection.

Experimental validation through 20,000 km endurance testing demonstrated ±2% torque tracking accuracy and stable autonomous operation over 1,559 hours. The test bench successfully generated field-representative failure modes including bearing pitting, chain guard fracture, and chain wear at realistic intervals—damage patterns unattainable with conventional constant-load protocols. The comprehensive MATLAB-based operator interface supports both manual investigation and automated long-duration campaigns. The demonstrated capability to reproduce realistic damage mechanisms under controlled laboratory conditions bridges the gap between simplified bench testing and expensive field trials, providing manufacturers with actionable durability data at reduced time and cost. Future work will extend the concept to three-dimensional radial loading, AI-based predictive maintenance, and musculoskeletal rider models. The biomechanical pedelec test bench is operational at Hochschule Aalen and available for collaborative drivetrain development programs.

ACKNOWLEDGEMENTS

This work was conducted in cooperation with daum electronic GmbH. The main idea and initial developments of the testbench is based on the research of Prof. Tillmann Körner of Aalen university. We would like to express our deepest gratitude for this. The authors also thank Jonas Huggenberger, Oezben Sarikurt, Moritz Paeslack and Jonas Seitz for their contributions to test bench development, instrumentation, and experimental execution. Special thanks to the workshop team, especially Günter Link, at Hochschule Aalen for mechanical fabrication support.

REFERENCES

[1] Zweirad-Industrie-Verband (ZIV), Market Data Reports, 2024, ZIV, www.ziv-zweirad.de/marktdaten/

[2] European Union, Regulation (EU) No 168/2013 on the approval and market surveillance of two- or three-wheel vehicles and quadricycles, Official Journal of the European Union, 2013.

[3] W. Petzke, "Muskelleistung und Wirkungsgrad beim Radfahren: Leistung der Gelenkbewegungen; Erklärung zum runden Tritt," Bundesinstitut für Sportwissenschaft, ISSN: 0341-7387, 2006.

[4] T. Körner, W. Daum, and A. Grimm, "Deflection-Test an Pedelec-Getrieben zur besseren Vorauslegung der Verzahnungstragbilder," Schweizer Maschinenelemente Kolloquium, Rapperswil, 2018.

[5] Schwarzer, S., Feldmann, S., Daum, W., & Körner, T. (2017). *Biomechanischer Pedelec-Prüfstand (BP-Prüfstand) zur besseren Verifizierung der Lebensdauer von Pedelec-Getrieben: Horizontale und vertikale Fahrmechanik – Tretmechanik – digitale Ansteuerung*, *AKAA*, 2020, ISBN 978-3-8440-7529-8

[6] J. Muetze and Y.C. Tan, "Electric bicycles - A performance evaluation," IEEE Industry Applications Magazine, vol. 13, no. 4, pp. 12-21, 2007.

[7] European Union, Regulation (EU) No 168/2013, Official Journal of the European Union, 2013.

[8] W. Petzke, "Muskelleistung und Wirkungsgrad beim Radfahren," Bundesinstitut für Sportwissenschaft, ISSN: 0341-7387, 2006.

[9] DIN 50100:2016-12, Load controlled fatigue testing - Execution and evaluation of cyclic tests at constant load amplitudes on metallic specimens and components.

[10] E. Haibach, Betriebsfestigkeit: Verfahren und Daten zur Bauteilberechnung, 3rd ed., Springer, 2006.

[11] EFBE Prüftechnik GmbH, "Test standards for bicycle components," Technical Documentation, 2020.
[12] F.E. Zajac, R.R. Neptune, and S.A. Kautz, "Biomechanics and muscle coordination of human walking," Gait & Posture, vol. 16, no. 3, pp. 215-232, 2002.
[13] J.P. Broker and R.J. Gregor, "Mechanical energy management in cycling: Source relations and energy expenditure," Medicine & Science in Sports & Exercise, vol. 26, no. 1, pp. 64-74, 1994.
[14] M. Andersson, B. Johansson, and A. Ståhl, "Hardware-in-the-loop simulation for powertrain development," SAE Technical Paper 2006-01-1495, 2006.
[15] A. Sivert, F. Betin, and J.-P. Bécar, "An Electrical Bike For Project Based Learning Platform," IEEE, 2011.
[16] A.R. Coggan and J.L. Ivy, "Muscle glycogen and the physiological determinants of endurance cycling performance," International Journal of Sport Nutrition, vol. 1, no. 1, pp. 1-28, 1991.
[17] Schramm, Dieter: Anthropomorphe Tutoren für Lernprozesse in mit Web 2.0-Technologie unterstützten Lehr-/Lernszenarien - Teilprojekt Perzeptionsbasierte Animation virtueller Charaktere - Abschlussbericht. Technische Informationsbibliothek u. Universitätsbibliothek 2014 Advanced Re-Engineering Approach in Humanoid Robot Development
[18] Feldmann, Sebastian: Advanced Re-Engineering Approach in Humanoid Robot Development, 2nd International Conference on Advances in Mechanical and Robotics Engineering, Schweiz, 2014, ISBN: 978-1-63248-031-6 doi: 10.15224/ 978-1-63248-031-6-143

Authors

Prof. Dr.-Ing. Sebastian Feldmann is Professor at Aalen University and founder of NectOne and co-founder of Sturm.Industries. He specializes in AI-based control theory, development of manufacturing solutions, robotics, and biomechanical Pedelec testing, leading the Metz E-PACKR 8.0 endurance testing project under guidance of Prof. Körner. Furthermore he was responsible for industrial research projects e.g. KIWeld (AI welding) and SimKI (simulation-based AI). As founder of GründerCampus Aalen, he promotes startups and teaches digitalization and control engineering.

M.Sc. Matthias Wiedenmann is a researcher from HS Aalen in cooperation with TU Dresden. He specializes in mechanical engineering with a focus on machine elements such as shafts, bearings and gears, individually and as a system. He worked on the engineering and design of the Metz G8 drive system and its testing / verification.